JOURNAL OF GEOPHYSICAL RESEARCH, VOL. 94, NO. D15, PAGES 18,495–18,514, DECEMBER 20, 1989

THE SHARAV CYCLONE: OBSERVATIONS AND SOME THEORETICAL CONSIDERATIONS

P. Alpert and B. Ziv

Department of Geophysics and Planetary Sciences
Raymond and Beverly Sackler Faculty of Exact Sciences
Tel Aviv University, Ramat Aviv, Israel

Abstract. A special study of the Sharav Cyclones indicates that they are the result of large-scale weak baroclinicity, enhanced by vigorous boundary-layer baroclinicity between the North African coast and the Mediterranean. It is illustrated how the jet stream plays a major role in the vertical circulation in producing a complex cyclonic circulation dominated by at least three mechanisms: large-scale interior baroclinicity, boundary-layer baroclinicity, and jet stream related circulations. The main characteristics of the Sharav Cyclone (also called the Saharan Depression or Khamsin Depression) in the Mediterranean are reviewed. Unlike the cold winter cyclone, the Sharav Cyclone is a spring cyclone. Its tracks lie mainly along the North African coast and turn to the north near the southeastern Mediterranean. Its warm front is active and is sometimes associated with extremely high surface temperatures. Its cold front is shallow. The Sharav Cyclone moves eastward relatively fast, typically faster than 10 m s^{-1}, and with a small speed variability. In general, there is an upper level trough to the west of the surface low and the surface horizontal scale is of the order of 500–1000 km. Finally, it is frequently associated with heavy dust/sand storms and low visibilities. Some of these features are illustrated in a case study of the April 28–30, 1986, cyclone. Vertical cross sections indicate a deep circulation associated with the exit region of an upper level jet. In addition to presenting evidence that the Sharav Cyclone is a deep tropospheric circulation, it is shown that the transverse indirect circulation at the exit region of the jet is a major component of its circulation. The classic two-level baroclinic model (Phillips, 1954) is applied. The effects of the major diabatic heating due to the sensible heat flux above the North African desert and the large north to south temperature gradients are incorporated through the thermal wind of the basic state. The model predicts the fast eastward motion, the relatively smaller horizontal scale and the fast growth rate. Furthermore, the model predicts an annual maximum growth rate in April and a secondary peak in October, which agrees with the frequency of occurrences of the Sharav Cyclones.

Paper number 88JD04228.
0148-0227/89/88JD-04228$05.00

1. Introduction

During winter the Mediterranean Sea region is influenced by mid-latitude cyclones which are associated with active weather, particularly in cold fronts. These cyclones are nearly absent during summer, when subtropical high pressure dominates the region. In the spring season, however, observations indicate the frequent occurrence of cyclones on the lee side and to the south of the Atlas Mountains. These cyclones generally move eastward along the southern coast of the Mediterranean Sea. Their source was identified by several investigators as lee cyclogenesis associated with the Atlas Mountains in Algeria [e.g., Weather in the Mediterranean, 1962]. This spring cyclogenesis is explained by the lee effect as well as by the coastal thermal gradient, which becomes quite large during spring, when the African continent's temperatures rise considerably relative to the yet cold sea [Pedgley, 1972]. The major role of the large north to south temperature gradient was first pointed out by Elfandy [1940]. The cyclogenesis initiated by the presence of an upper level trough is the source of the "Sharav Cyclones," sometimes referred to as the "Saharan Depressions" or "Khamsin Depressions." There is also a manifestation of cyclogenesis along the Libyan and Egyptian coasts. The cyclones, which originate in the lee of the Atlas Mountains, move more or less along the coastal line. Sometimes the cyclones are formed along the coast, primarily during the spring season. Pedgley [1972] discusses the low variability in the frontal structure and has associated this with characteristics of the North African coast and, in particular, the strong heating above land.

Although it is a major synoptic feature of the Mediterranean region, relatively few studies of the Sharav Cyclone have been made. Most of them are basically case studies done by local synopticians [Elfandy, 1940; Tantawy, 1964; Pedgley, 1972; Winstanley, 1972; Druyan, 1978]. Tantawy [1964] has suggested that the activity of these cyclones is strongly correlated with the subtropical jet stream and sometimes, in severe weather events, with the southward transition of the polar jet stream.

Earlier studies suggest that the coastal baroclinicity in spring has a major impact upon the Sharav Cyclones. However, to the best of our knowledge, this effect has not yet been incorporated in any dynamical model of these cyclones.

In the present study we first review (section 2) the main features of the Sharav Cyclone compared to the winter cyclones and then follow with a recent case study from spring 1986. In section 3 a two-level baroclinic model which includes diabatic heating effects is applied to the North African coast in an attempt to explain some of the Sharav Cyclone's unique features. The use of some assumptions (section 4) becomes inevitable owing to the sparsity of the data above the Mediterranean Sea and North Africa. Finally, in sections 5 and 6 the results are discussed and then summarized.

2. The Sharav Cyclone: Main Features

1. The Sharav Cyclone is primarily characteristic of the spring season. Figure 1a [from Reiter, 1975] demonstrates the occurrence of cyclogenesis in the Mediterranean Sea region in autumn (September-November), winter (December-February) and spring (March-May). Each point represents the first occurrence of a cyclone during a 7-year period. Areas which are well populated with these points are regarded as cyclogenetic. In addition to the expected cyclogenesis over the Mediterranean Basin, especially in winter, we can see a very intensive cyclogenetic center on the lee side of the Atlas Mountains in the spring chart. For the area map, see Figure 1b. Another, weaker cyclogenetic region is seen in the coastal zone of east Libya and Egypt.

2. The Sharav Cyclone's track is typically close to the North African coast and in general not over the Mediterranean, as for the marine-type track of the winter cyclones. This point will be demonstrated later for the spring of 1986.

3. The Sharav Cyclone has an active warm front. It differs from the winter cyclones, which are characterized by active cold fronts with primarily convective cloud cells. Figure 2 is a typical example of the cloud structure of a Sharav Cyclone on April 23, 1986, at 1650 UT. For comparison, Figure 3 shows the cloud structure of a typical winter cyclone at approximately the same longitude on January 7, 1986, at 0130 UT. Cross sections through the warm front in the following case study will show the intensity of the updraft and circulation (Figure 10).

4. The temperatures in the warm sector are remarkably high. Figure 4 shows the frequency distribution of the April daily maximum temperature in Cairo, Egypt [Tantawy, 1969]. The graph is a composite of two nearly Gaussian shape curves: the main peak belongs to the "normal" days with maritime air mass influence, while the secondary peak is the result of the Sharav events. The distance between the two peaks is about 7°-8°C.

5. The cold front is shallow but well defined near the surface. The surface temperature drop across the cold front is very sharp and has typical values of 10°-20°C, [e.g., Elfandy, 1940]. On the other hand, the depth of the cold air mass is only 1-2 km in most of the Sharav Cyclone events. Hence the cold front is generally not associated with well-developed clouds nor with any precipitation [Tantawy, 1964].

6. The cyclone moves eastward relatively fast. While the average speed of the winter cyclones in the Mediterranean is about 5° longitude per day (about 5.5 m s^{-1}) and this value may vary considerably, the Sharav Cyclones move at about twice that speed (~10 m s^{-1}) and their speed variability is quite low.

7. The Sharav Cyclone is associated with an upper level trough far to the west. Although its central pressure on the surface chart is comparable to that of the Mediterranean cyclones, closed contours appear only in the lower levels of the troposphere, and in general, the 500-mbar trough is further to the northwest. This will be illustrated in the following section in the Sharav Cyclone study (see Figure 9).

8. The horizontal size of the cyclone is 500-1000 km, as opposed to over 1500 km for the winter cyclones.

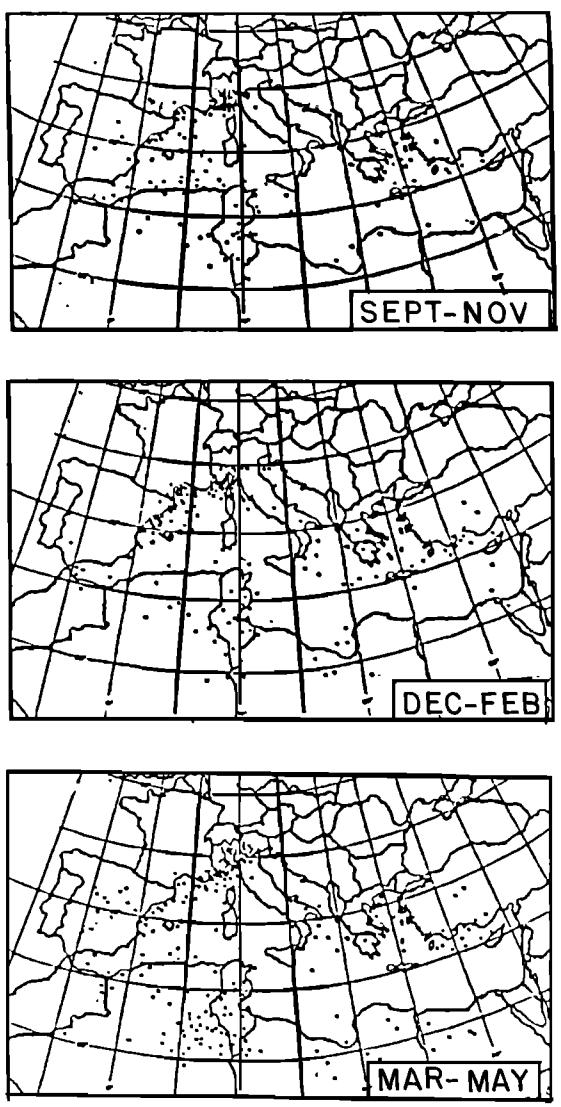

Fig. 1a. Occurrence of cyclogenesis in the Mediterranean during the seasons indicated for January 1, 1965, through December 31, 1969, and October 1, 1972, through July 31, 1974, for autumn, winter, and spring [after Reiter 1975].

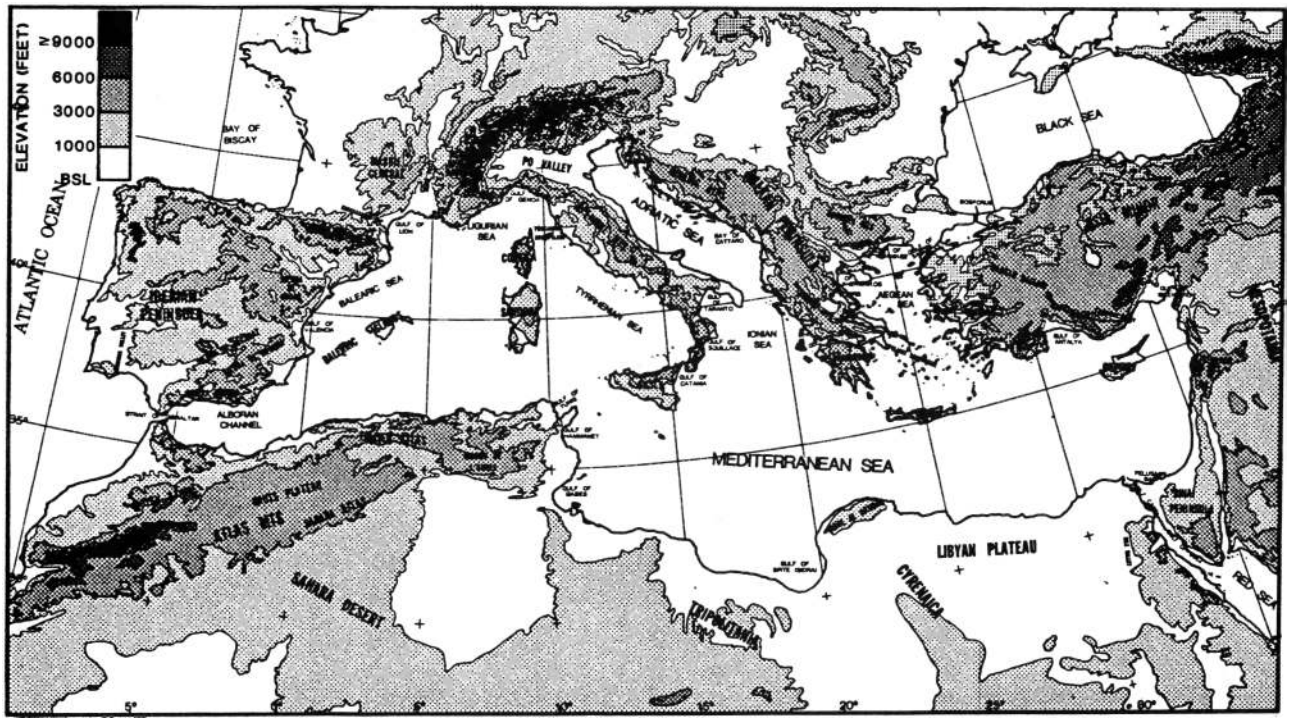

Fig. 1b. Topography of the Mediterranean area [from Reiter, 1975].

9. The cyclone path tends to follow the North African coastal line and when approaching Sinai (southeastern Mediterranean) it sometimes turns to the north, following the direction of the eastern Mediterranean coastline. Figure 5 summarizes the tracks of 10 Sharav Cyclones which were observed to pass through the Egyptian coast during the 1986 spring season (March-May).

10. The passage of a Sharav Cyclone is frequently typified by heavy sandstorms and dust storms in the Mediterranean region, associated near the surface particularly with the cold front. The dust, which is associated with the warm front and the warm sector, may reach the 500-mbar level and above. The influence of the Sharav Cyclone goes far beyond regional interest because of the

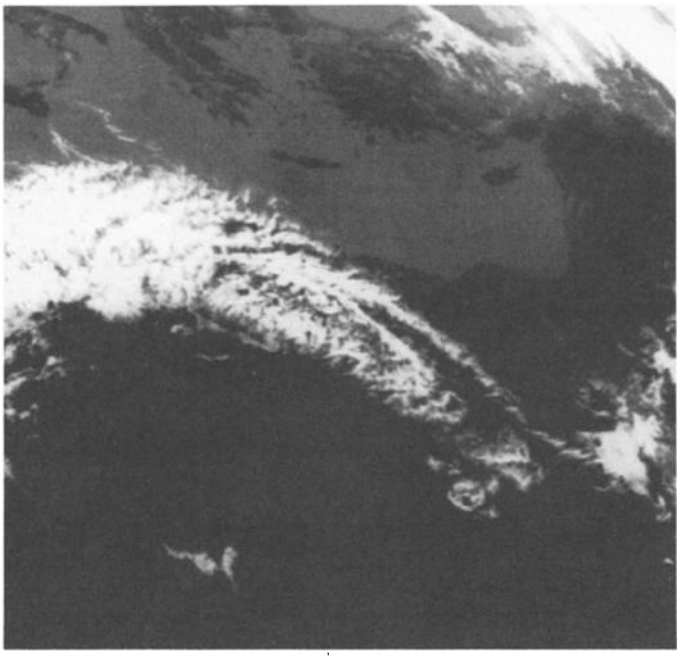

Fig. 2. IR satellite (Meteosat) picture of the Sharav Cyclone in the Bay of Sidra on April 23, 1986, at 1650 UT.

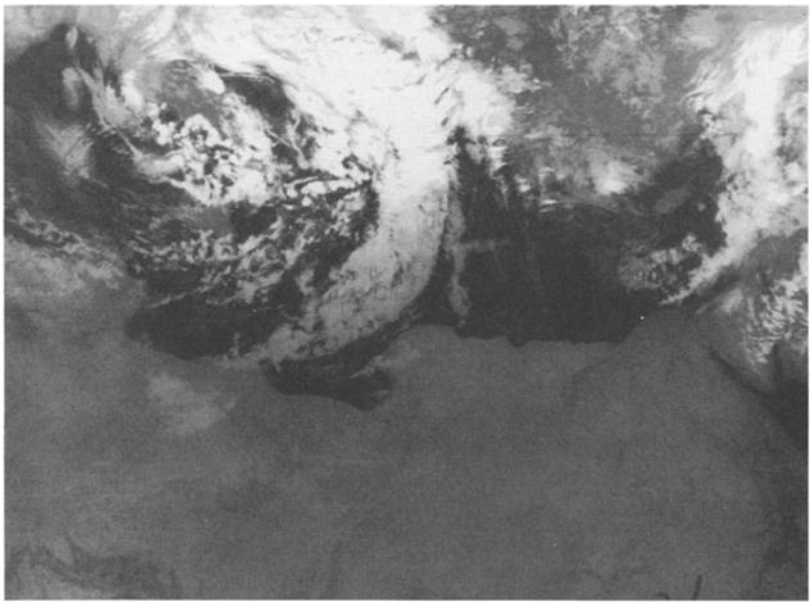

Fig. 3. IR satellite (NOAA 9) picture of a cold winter cyclone on January 7, 1986, at 0130 UT.

huge amounts of dust transported to large horizontal distances [e.g., Lee, 1983; Westphal et al., 1985].

Table 1 summarizes the major differences between a typical cold winter cyclone and the Sharav Cyclone. Table 1 is based upon the aforementioned literature and, in particular, on Weather in the Mediterranean [1962], Reiter [1975], and recent satellite and synoptic studies by the authors. Horizontal scale and surface depth are determined by the closed isobars at the surface. The time scale is derived from the horizontal length scale and the speed of the cyclone.

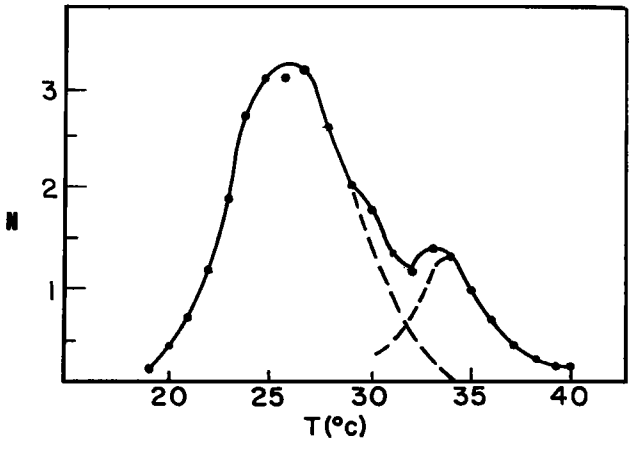

Fig. 4. Frequency distribution with 1°C intervals of the April daily maximum temperatures in Cairo, Egypt [after Tantawy, 1969]. The number, N, indicates average number of days. Dashed curves represent approximate extension to Gaussians (see text).

3. A Sharav Cyclone on April 28-30, 1986

On April 28, 1986, at 1200 UT, an upper level cyclone dominated the western Mediterranean (Figure 6a). On the surface chart (Figure 6b) at that time, the primary cyclone was in Italy and a "Sharav Cyclone" moved along the North African coast (Figure 7). Although we ourselves performed the analyses, we also used the European Centre for Medium-Range Weather Forecasting (ECMWF) analyses to complement our maps where data were insufficient. It was found that the ECMWF analyses do capture the Sharav Cyclone realistically, although the forecasts are generally poor. On April 29, the Sharav Cyclone reached the Nile delta in Egypt, and temperatures in the warm sector exceeded 38°C. The eastern Mediterranean became covered by medium-level clouds, which can be clearly seen in the IR Meteosat image from April 29, at 1200 LST (1000 UT); see Figure 8. Dust storms were reported in eastern Egypt.

The synoptic charts at 500 mbar and at the surface (see Figures 9a and 9b) do not show a major change in the upper level conditions; the primary upper level low is still in Italy (compare Figures 6a and 9a), but the 500-mbar wind at Bet-Dagan, Israel, veered from weak northwesterly (~5 knots, or ~9 km h^{-1}) to a stronger westerly wind of 25 knots (~45 km h^{-1}). A similar veering, with stronger winds, is noticed in the 300-mbar chart (not shown). At the surface, however, as may be seen by comparing Figures 9b and 6b, the

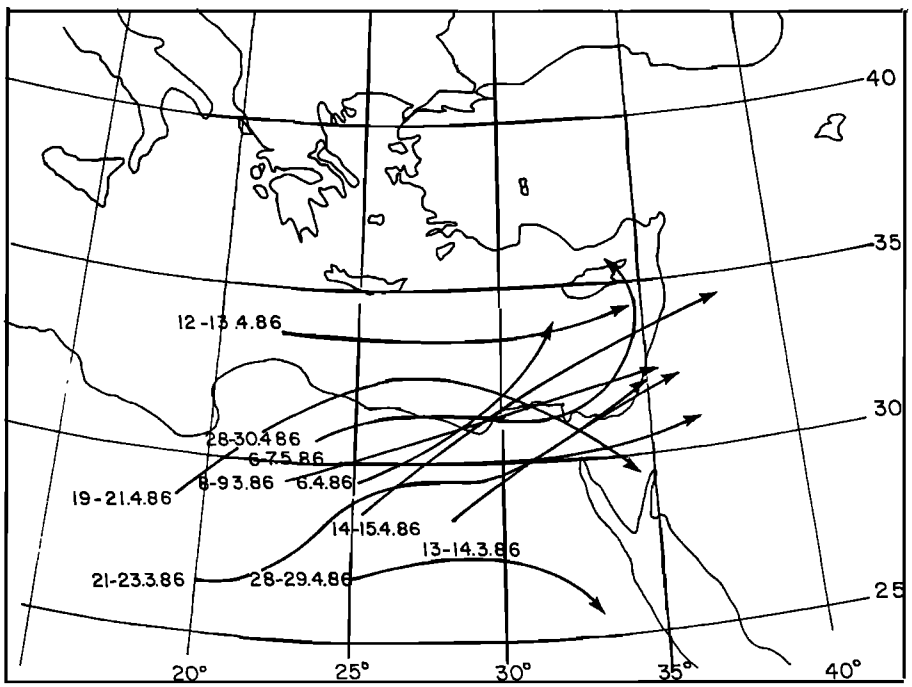

Fig. 5. Trajectories of 10 Sharav Cyclones that passed Egypt during spring 1986 (March-May).

Sharav Cyclone has traveled a long distance of about 1000 km, that is, about 9° latitude in 1 day. Although the primary trough in Figure 9a is still far to the west, at about 15°E longitude the intensification of the upper level flow and the strong diffluence at the upper levels in the Sinai Peninsula region seem to play a role similar to that of an exit region of a jet streak, as discussed by Brill et al. [1985]. Also, one can notice (see Figure 9b) that severe dust storms reduced visibilities below 3 km in eastern Egypt, surface winds exceeded 20 knots (~36 km h^{-1}), and temperatures dropped from 38° to 22°C across the cold front from Cairo to Alexandria (a distance of about 100 km).

The possible role of the transverse indirect circulation at the exit region of an upper level jet in the generation and maintenance of the Sharav Cyclone, and perhaps the weather associated with it, is quite difficult to study because of the lack of sufficient upper air data above the North African coast. Fortunately, as the cyclone approaches the southeastern corner of the Mediterranean, as on April 29, 1986, at 1200 UT, a northwest to southeast cross section along the right portion of the Sharav Cyclone (see Figure

TABLE 1. Summary of Cyclone's Features for the "Sharav Cyclone' and the Winter Cyclone in the Mediterranean Region

Cyclone Feature	Sharav Cyclone	Winter Cyclone
Generation region and track	lee of Atlas Mountains North African Coast	Gulf of Genoa and Mediterranean
Horizontal scale, km	<1000	>1500
Vertical scale, km	<3-5	full troposphere
Time scale, days	0.5-1	1-4
Speed, m s^{-1}	>10, with small variability	~5, frequently with large changes of speed
Surface depth, mbar	~10	10-20
Dominant cloud type	warm front (medium- and high-level clouds)	cold front (convective low-level clouds)
Surface temperature gradients in the cold front, K/100 km	10-20	<5-10
Main season	spring	winter

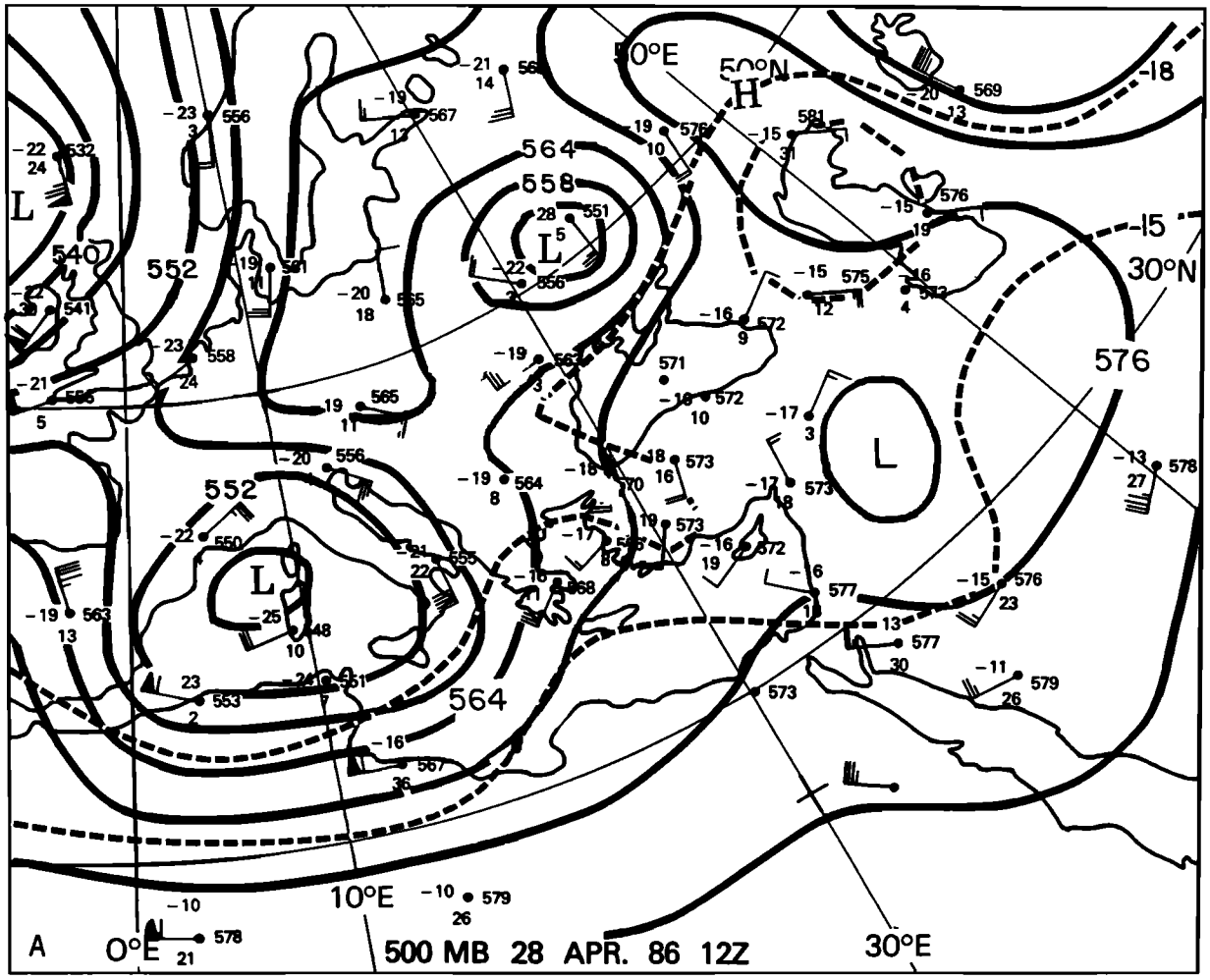

Fig. 6. Synoptic charts for the Mediterranean region on April 28, 1986, at 1200 UT; (a) 500-mbar isohypses and isotherms (dashed curves) with intervals of 6 dm and 3 K; (b) surface isobars, contour interval of 2.5 mbar. Dashed line in Figure 6b indicates the cross section for Figure 11. Visibility is indicated according to the WMO code for synop, that is, up to 50 in hectometers and above 55 by kilometers, when subtracting 50.

9b) did contain some relatively close radiosondes. Figures 10a and 10b present the cross sections along the line from (left) 50°N, 20°E to (right) 20°N, 40°E, taken from the ECMWF analysis for potential temperature, tangential wind vectors, and the normal component of the horizontal wind, with a contour interval of 5 m s^{-1}, positive into the page (Figure 10a), and relative humidities, in percent (Figure 10b). The calculation of the vertical velocity ω follows the routine ECMWF analysis, in which the horizontal divergence is integrated from the surface to the corresponding level. The ω analysis also includes the coordinate correction $V_H \cdot \nabla p$ [e.g. Holton, 1979, p. 72].

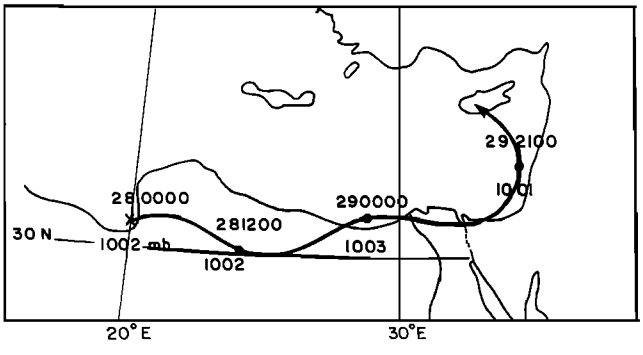

Fig. 7. Track of the Sharav Cyclone on April 28-29, 1986. The numbers above the track indicate date and hour (UT), while below the track the central surface pressure is depicted.

The point at the surface warm front (~32°N, 32°E), at the southern Mediterranean border, is quite close to the cyclone center and gets the strongest upward motion of about 0.7 Pa s^{-1}. The maximum vertical velocities are at 600-400 mbar and correspond well with the massive medium level cloud cover reported there (compare Figures 10a and 10b). Above 300-400 mbar, vertical velocities decrease considerably and the transverse diverging flow to the south intensifies. There are two jets; the stronger one (30 m s^{-1}) right above the southern Mediterranean at about 200 mbar, which is probably associated with the upper level polar jet, while the higher (100 mbar) and more southern jet (22°N) is to be identified as the subtropical

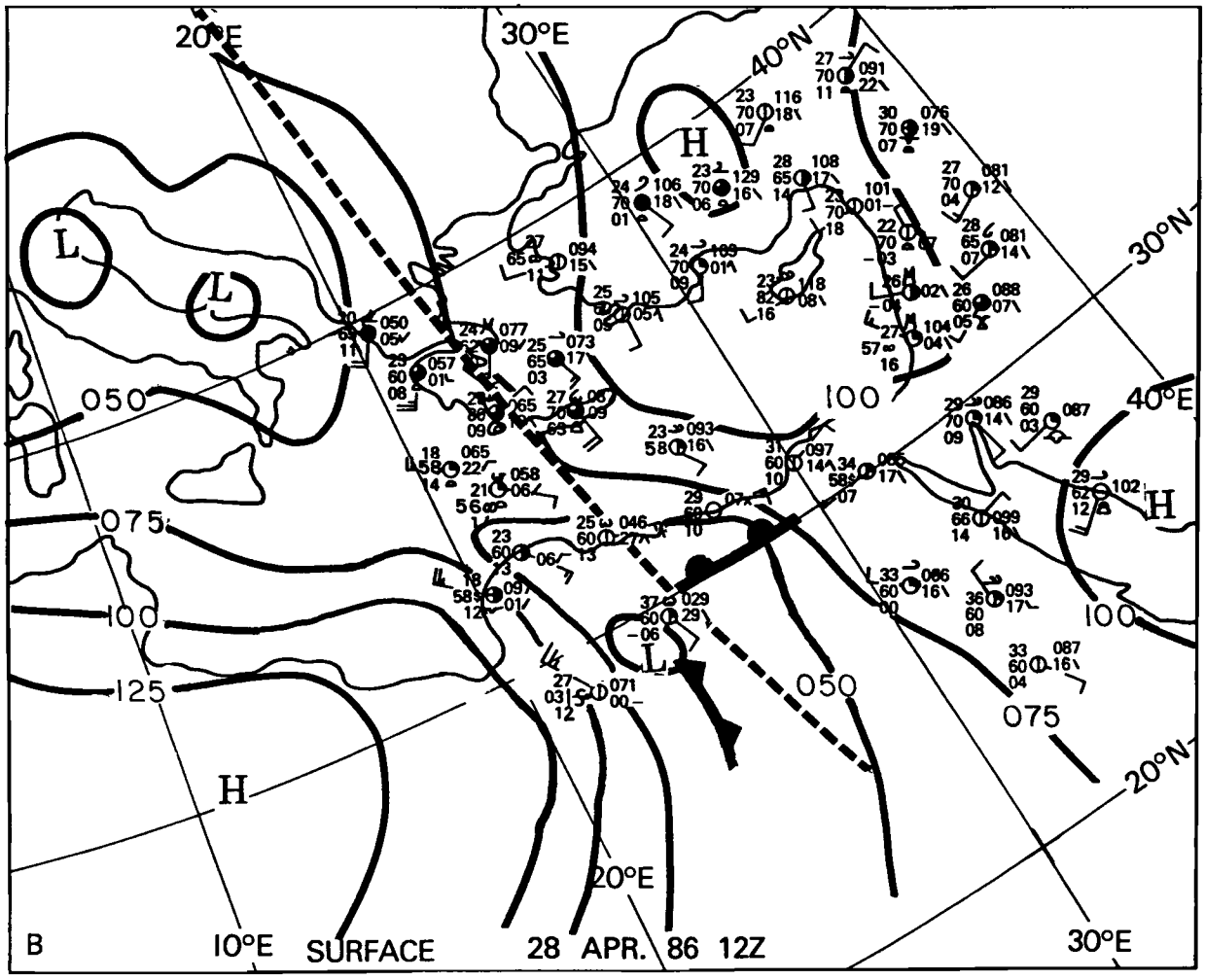

Fig. 6 (continued)

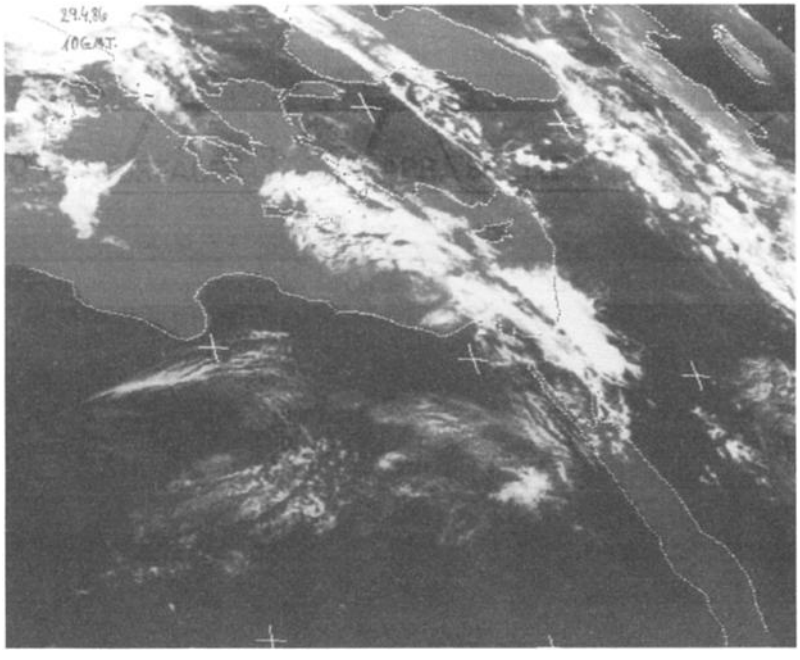

Fig. 8. IR satellite (Meteosat) picture for April 29, 1986, at 1000 UT.

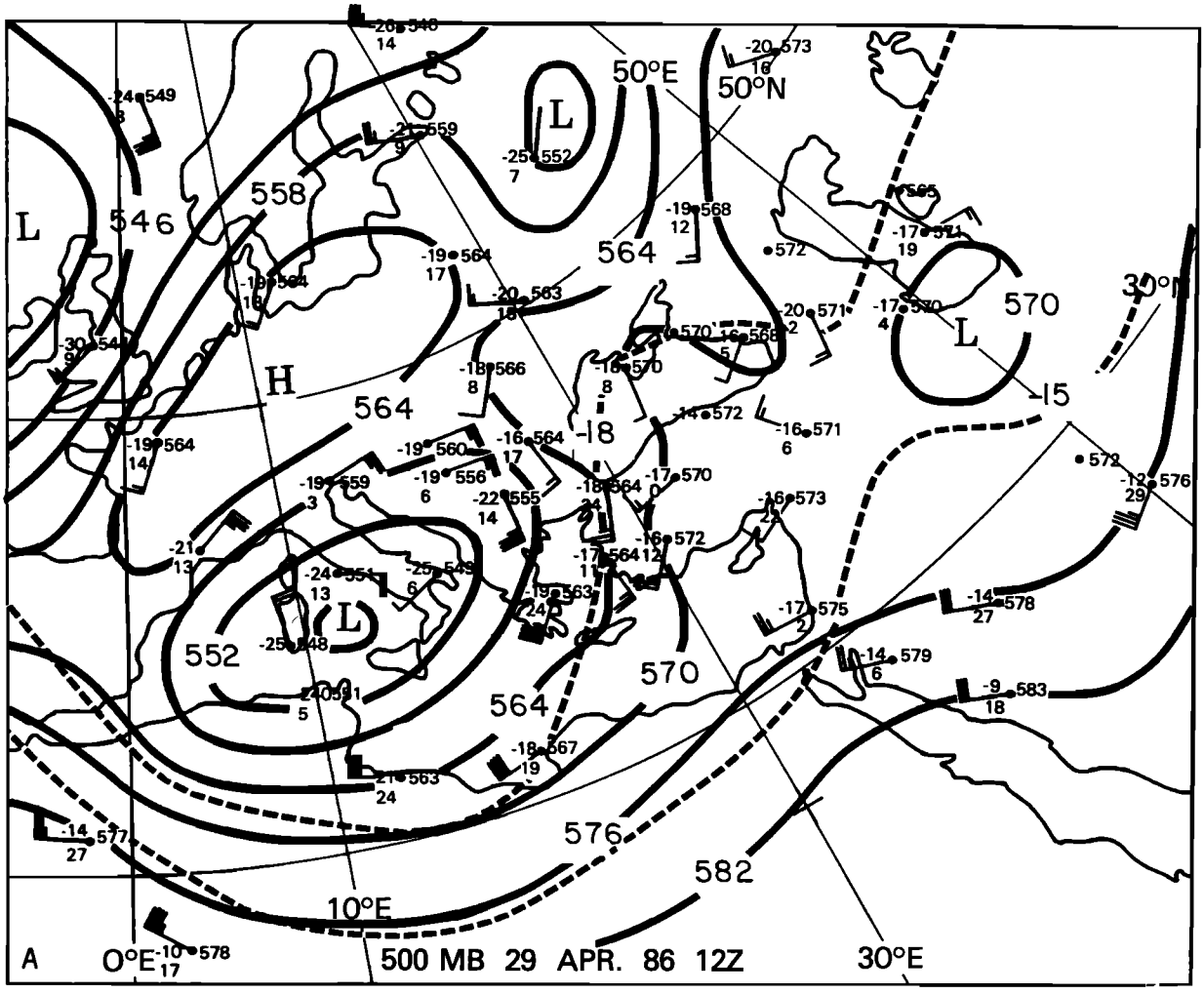

Fig. 9. As in Figure 6, but for April 29, 1986, at 1200 UT. Dashed line in Figure 9b indicates the cross-section line for Figure 10.

jet. The approximately transverse indirect circulation in the exit region of the former corresponds well with that reported and simulated by Brill et al. [1985] in North America, with deep and precipitating cyclones. In the present study the dryness of the planetary boundary layer and the lower troposphere up to about 2-3 km (see Figure 10b) nearly inhibits surface precipitation and the most commonly observed cloud was a well-developed altocumulus with medium-altitude bases at about 3 km.

It is of special interest to compare the vertical cross sections for April 29, at 1200 UT, with those 24 hours earlier in approximately the same position relative to the Sharav Cyclone. Figures 11a and 11b present the cross sections for April 28, 1986, at 1200 UT, corresponding to Figures 6a and 6b. The dashed line in Figure 6b indicates the cross-section line. As mentioned earlier, the conventional synoptic data coverage above the North African coast is insufficient. However, the high similarity obtained between these cross sections and those for April 29 seem to indicate the important contribution of unconventional data, like satellite winds and temperatures, that is incorporated routinely in the ECMWF analyses [Bengsston et al., 1982]. The cross sections are very similar to those 24 hours later in many of the details: (1) The surface centers of the Sharav Cyclone (indicated by letter I in Figures 10a and 11a) are located right beneath the jet streak (see letter L in Figures 11a and 10a). (2) A very dry layer from 950 to 800 mbar exists, and on top of it there is a massive medium-level cloud (Figures 11b and 10b). (3) The maxima of the upward motion are above the cyclone, with the upper maximum at the level of 500 mbar (Figures 11a and 10a).

These indicate that the Sharav Cyclone has kept its basic structure throughout the 1000-km track along the North African coast. There are, however, some important changes, as follows: On April 28 the northern colder cyclone (the Genoa Cyclone) is much closer to the Sharav Cyclone. Notice the strong upward motion (Figure 11a), which is located at 42°N compared to 48°N on April 29 (Figure 10a). It is also strongly pronounced in the two tranverse circulations, which are

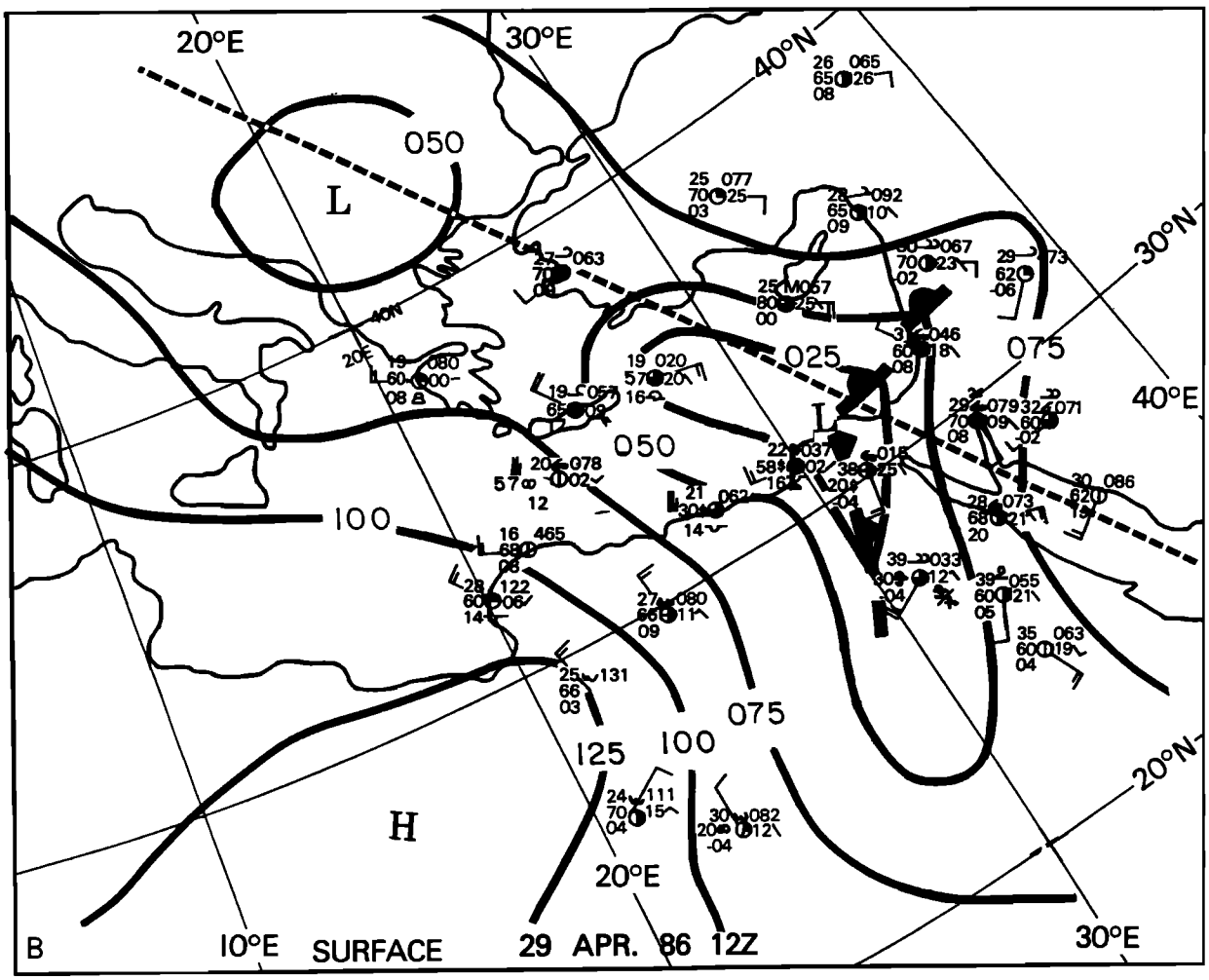

Fig. 9 (continued)

nearly combined for the two cyclones on April 28 (Figure 11a) but are separated on April 29 (Figure 10a). The two cyclones are closer on April 28, even though the jet streak associated with the Sharav Cyclone is further to the south, whereas on April 29 the jet streak is right above the coastline. This seems to indicate a tendency of the Sharav Cyclone to gradually cut off from the parent Genoa Cyclone. This process may also be associated with the lowering of the center of the transverse circulation from 550 to 700 mbar (the centers are indicated by the letter I). Furthermore, it is possible that in the earlier stages the Sharav Cyclone is primarily supported by the synoptic baroclinicity induced by the northern trough, while in the later stages, other mechanisms like jet streak effects and/or lower-level baroclinicity take place. Of course, the evidence from one case is not sufficient for making further conclusions because the differences between the two stages as well as the different topographical cross sections might contribute to the aforementioned changes.

Another difference between the two cross sections is the stronger upward motion on April 29. Again, this difference as well could be the result of insufficient upper level data in the area of concern, which is particularly noticed on the April 28 maps (Figures 6a and 6b).

On the evening of April 29 the cyclone turned toward the north (see Figure 7), passed through the Israeli coastline, and reached the Cyprus Island region. The passage of the cold front in Israel was associated with wind gusts of 25–30 knots (~45–54 km h^{-1}) and local dust storms in the Negev Desert of Israel. On the next day, April 30, the southeastern Mediterranean region became influenced by maritime cool air. The temperature sounding of Bet Dagan, Israel, at 1200 UT on April 30, versus that of 24 hours earlier, illustrates the cool and shallow air mass penetration that took place as the cold front passed the station. The depth of this cold layer is only about 1.5 km (Figure 12).

The current case could be classified as a slightly deeper and more pronounced cyclone than the typical Sharav Cyclone described in section 2, whose features were summarized in Table 1. The surface depth was about 10 mbar and the horizontal and vertical scales were close to those given in Table 1. However, higher than typical surface temperature gradients were observed (see Figure

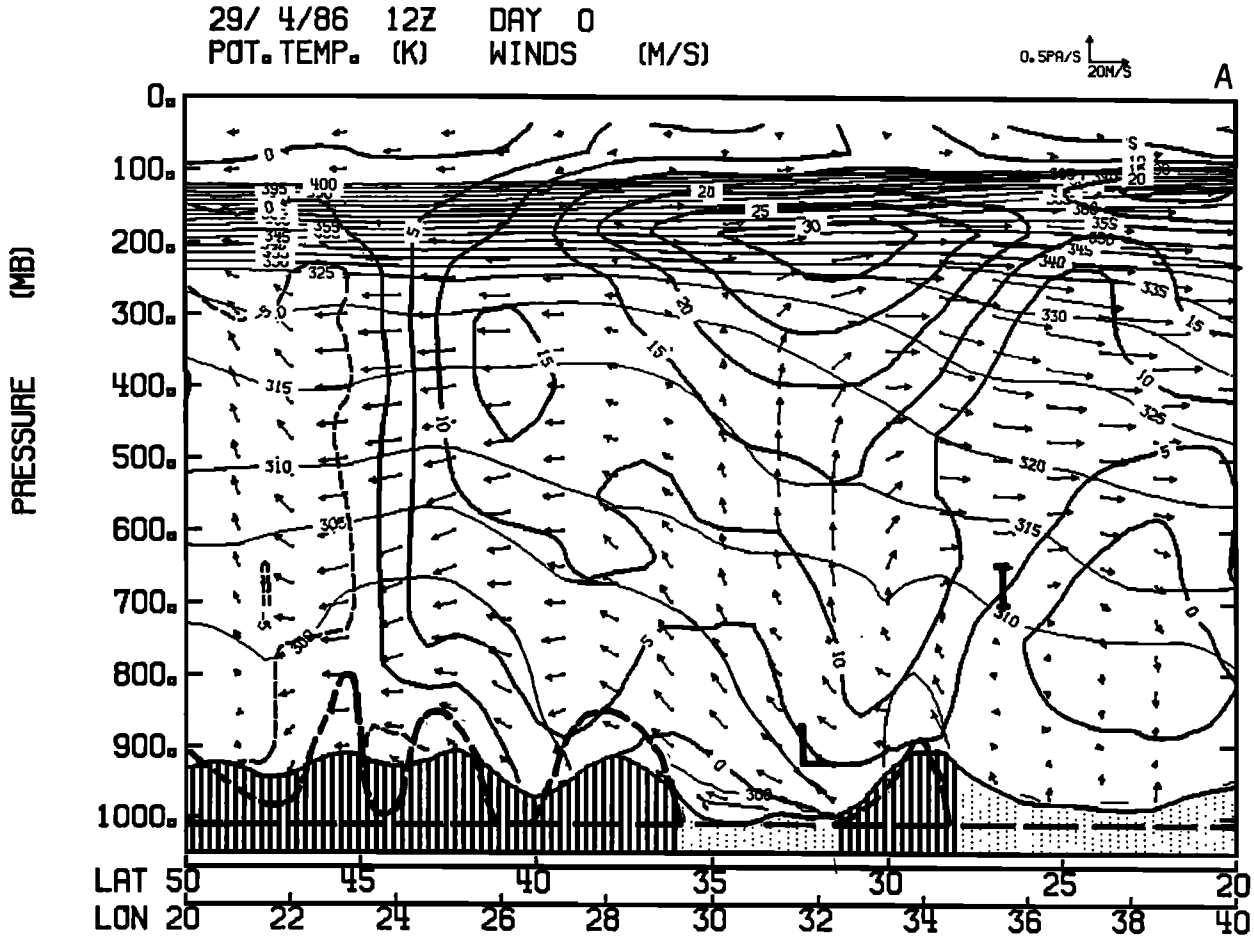

Fig. 10. Cross sections for April 29, 1986, at 1200 UT, extending along a line from 50°N, 20°E (left) to 20°N, 40°E (right) from the ECMWF analysis. (a) The potential temperature (contour interval 5 K), tangential wind vectors (scale at the upper right-hand corner), and the normal component of the horizontal wind (contour interval of 5 m s^{-1}, positive into the page). (b) The relative humidity (in percent). In Figure 10a, isentropes 300 and 305 K were subjectively smoothed to remove false super-adiabatic layers in the analysis. The line and dot shading signifies the land and ocean in the ECMWF model. The heavy dashed curve indicates the real topography. The geographic location of the cross section is indicated in Figure 9b.

9b) and relatively stronger dust storms were reported. The classification was based upon the analysis of all 10 Sharav Cyclones that were observed during spring 1986.

4. The Model

4.1. The Model Equations

The two-level baroclinic model that was originally suggested by Phillips [1954] to study baroclinic instability is employed here, and the effects of diabatic heating upon the basic state are investigated. Our basic approach is to examine, as a first step, whether we can obtain from the two-layer model at least a zero-order approximation for the dynamics of the Sharav Cyclone. This was based on the assumptions that quasi-geostrophic dynamics can handle a disturbance of small horizontal scale and that the linear model is sufficient at this basic level.

The model levels are illustrated in Figure 13. The upper level, level 0, was chosen to be 400 mbar, while level 4 is at the 1000-mbar level. The "omega" vertical velocity in the isobaric coordinate system was assumed to be zero at the upper and lower levels. Actually, according to the case study discussed in section 3, the 300- or even 200-mbar surface might better fit the top boundary condition of zero vertical velocity, but even in that case, the drastic reduction in the vertical velocities starts well below 400 mbar. Also, in a recent analysis of a few additional cross sections of Sharav Cyclones (e.g., March 22, 1986), the upward motion became close to zero near the 400-mbar level.

The quasi-geostrophic vorticity equations at levels 1 and 3 and the thermodynamic equations for level 2 are

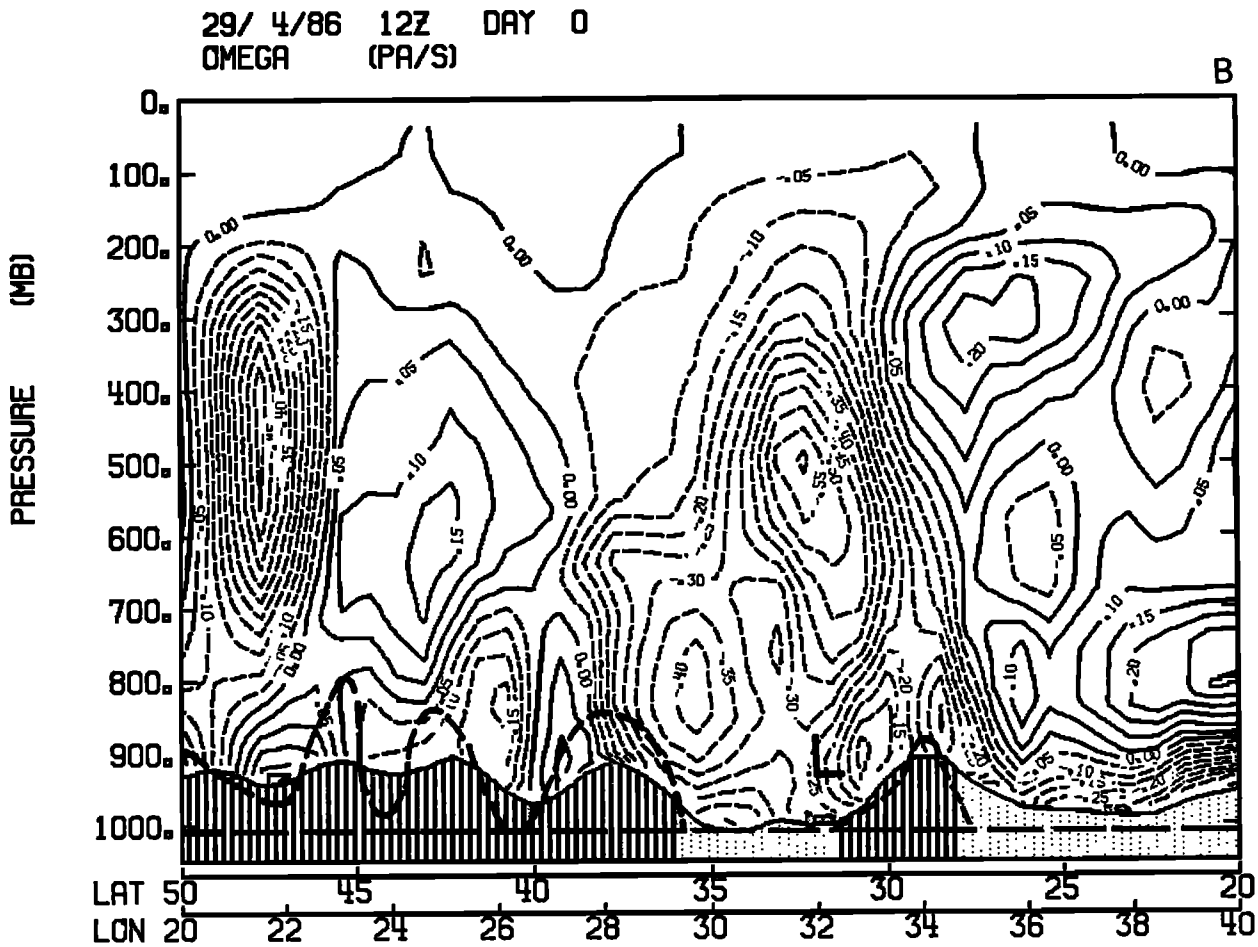

Fig. 10 (continued)

$$\frac{\partial \xi_i}{\partial t} + \underline{V}_i \cdot \nabla(\xi_i + f) = f_o \left(\frac{\partial \omega}{\partial p}\right)_i \qquad i = 1,3 \quad (1)$$

$$\frac{\partial}{\partial t}\left(\frac{\partial \phi}{\partial p}\right)_2 + \underline{V}_2 \cdot \nabla\left(\frac{\partial \phi}{\partial p}\right)_2 + \sigma\omega_2 = \left(-\frac{\alpha}{c_p}\frac{Q}{T}\right)_2 \qquad (2)$$

where

ξi	vorticity at level i;
T	temperature;
f	Coriolis parameter;
f_o	constant Coriolis parameter;
$\underline{V}_i$	wind vector at level i, $k x \nabla \psi_i$;
ψ_i	stream function at level i, ϕ_i/f_o;
ψ	geopotential height.

$$\sigma = -\frac{\alpha}{\Theta}\frac{\partial \Theta}{\partial p}$$

where

Θ	is the potential temperature;
α	$1/\rho$;
Q	diabatic heating;
c_p	specific heat at constant pressure;
ω	vertical p velocity, dp/dt.

The explicit contribution of the diabatic heating Q was not incorporated in (2), but its effects on the static stability parameter and on the thermal wind were estimated and introduced in the model. The justification for this procedure is investigated in section 4.2.

Equations (1) and (2) are numerically formulated and then linearized over a basic state, which consists of a constant zonal flow U_1 and U_3 at levels 1 and 3, respectively. Next, we applied the aforementioned boundary conditions for "omega" and inserted wave solutions for the perturbation quantities. The solution for the phase speed c is then found to be (see for example, Holton [1979])

$$c = U_m - \frac{\beta(k^2 + \lambda^2)}{k^2(k^2 + 2\lambda^2)} \pm \delta^{0.5}$$

where

$$U_m = \frac{1}{2}(U_1 + U_3), \quad \lambda^2 = f_o^2/\sigma\Delta p^2$$

$$\delta = \frac{\beta^2\lambda^4}{k^4(k^2+2\lambda^2)^2} - U_T^2\frac{2\lambda^2 - k^2}{2\lambda^2 + k^2} \qquad (3)$$

$$U_T = \frac{1}{2}(U_1 - U_3), \quad \beta \equiv \frac{\partial f}{\partial y}$$

where σ is the static stability parameter, and $k=(2\pi)/L$ is the wave number. U_m and U_T are the vertically averaged zonal wind and the basic state thermal wind for the interval $\Delta p/2$, respectively.

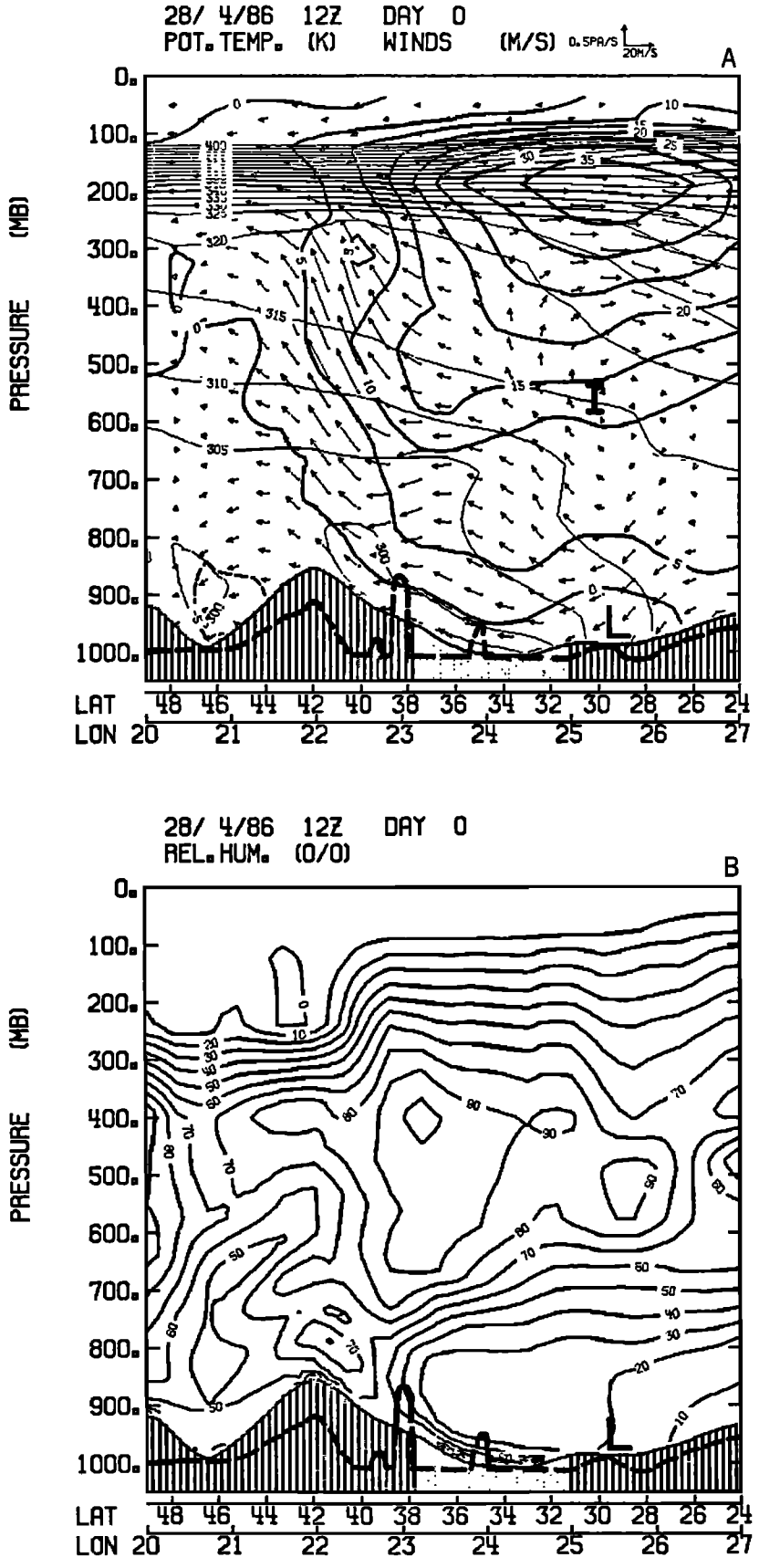

Fig. 11. Same as Figure 10, except for April 28, 1986, at 1200 UT, and along the line from 49°N, 20°E (left) to 24°N, 27°E (right). The geographic location of the cross section is indicated in Figure 6b.

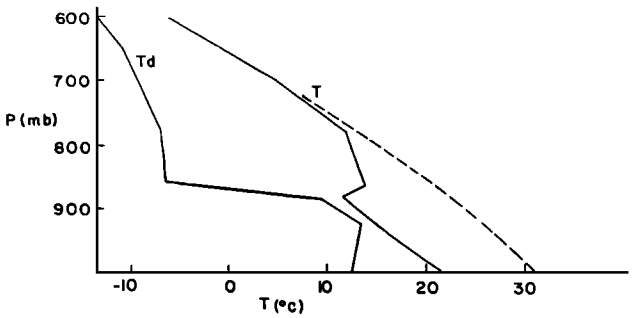

Fig. 12. Temperature and dew-point soundings (solid curves) for April 30, 1986, at 1200 UT, and temperature sounding for April 29, 1986, at 1200 UT (dashed curve), at Bet-Dagan, Israel (Station 40179).

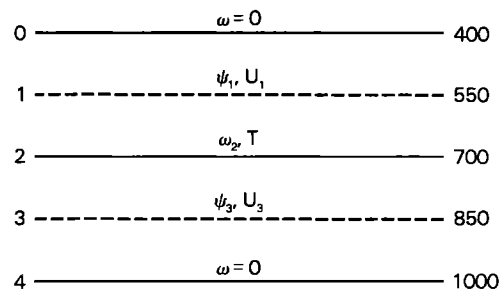

Fig. 13. Scheme of model levels.

The real part of c defines the phase speed of the cyclone, while $k(-\delta)^{0.5}$ is the growth rate, for $\delta < 0$. For positive δ, solutions are stable.

Substituting for δ into the growth rate expression and differentiating with respect to k, the wave with maximum growth rate k_{max} is obtained, as

$$k_{max}^2 = y\lambda^2 \tag{4}$$

where y is the solution of the fifth-order polynomial

$$y^5+6y^4+4y^3-8y^2-(12/c_o^2)y-8/c_o^2 = 0 \tag{5}$$

and where

$$c_o^2 = (2\lambda^2 U_t/\beta)^2 \tag{6}$$

For a given thermal wind U_T, a static stability σ ($\lambda^2=f_o^2/\sigma\Delta p^2$), and β, (6) determines c_o. Hence the solution of (5) for this value of c_o defines the wave number k_{max} with the maximum growth rate. The maximum growth rate γ_{max} could be shown to be

$$\gamma_{max} = \frac{\beta}{2\lambda(2+y)}\left(\frac{-c_o^2y^4+4c_o^2y^2-4}{y}\right)^{1/2} \tag{7}$$

and the phase speed c_{max} is

$$c_{max} = U_m - \frac{\beta}{\lambda^2}\frac{(y+1)}{y(y+2)} \tag{8}$$

For the neutrality curve one finds that $c_o^2 = 1$, for which $y=2^{0.5}$ becomes the solution to (5), leading, as expected, to a growth rate of zero. The critical vertical wind shear associated with $c_o = 1$ was shown to correspond well with the observations of averaged horizontal temperature gradients due to the baroclinic adjustment process, as suggested by Stone [1978]. But, in our case, that is, subtropical latitudes in spring, the baroclinic adjustment is not efficient [Stone, 1978]. Consequently, the maximum unstable modes were calculated from the observed monthly averages, yielding c_o values which are smaller than 1.

4.2. Modification of the Basic State Due to Diabatic Heating

The application of the two-level model requires the calculation of temperature tendencies at the 700-mbar level. The amount of the radiative diabatic heating Q at this level is of the order of 1 K d^{-1}; see, for example, the estimation by Ackerman and Cox [1982, p. 9000] for similar conditions in the Saudi-Arabian heat low. In contrast, the horizontal temperature advection, for instance, is estimated to be 1 order of magnitude higher. Taking a typical horizontal temperature gradient of 5 K per 500 km and a wind speed of 10 m s^{-1}, a temperature tendency of ~10 K d^{-1} is obtained.

Although the radiative heating is relatively small in a nondusty atmosphere, the diabatic heating contribution by the large sensible heat fluxes in the desert boundary layer cannot be neglected. Ackerman and Cox [1982], for instance, have estimated this contribution to be as high as 4.2 K d^{-1} in the 1000- to 800-mbar layer over the Saudi-Arabian desert.

In section 5 the climatological data from Cairo, Egypt, will be employed to calculate the mean velocity U_m, the thermal wind U_T, and the static stability parameter. The values of f and β are for the latitude of 30°N. On the substitution of these input values in (7) and (8), the speed and maximum growth rate for the perturbation could be calculated. However, the climatological data consist of two very different stages of the North African lower troposphere. The first is a precyclone phase, in which the boundary layer is gradually heated by both advection and surface heat flux. In the second stage the lower troposphere cools appreciably, as shown in Figure 12. In order to take into account the appropriate precyclonic background as a basic state, the contributions of diabatic heating to the thermal wind U_T and to the static stability parameter σ will be estimated.

4.2.1. Calculation of the sensible heat flux contribution. In the following discussion the source of the sensible heating is assumed to be due solely to the absorption of solar radiation at the surface. Let $\beta(\theta)$ represent the atmospheric

transmissivity at the zenith angle θ, and A represent the surface albedo; then the amount of solar energy absorbed in a surface unit area per second at latitude θ at the date the Sun makes an angle δ and at the hour in which the Sun inclination is h, is [e.g., Liou, 1980]

$$I_o\beta\ (1-A)\cos\theta =$$

$$I_o\beta\ (1-A)\ [\sin\phi\ \sin\delta + \cos\phi\ \cos\delta\ \cos\mu]$$

where I_o is the solar constant. The total daily amount of available solar energy S at the surface is then obtained by a diurnal integral of this expression. The integral was performed assuming a desert albedo of 0.3, following Rockwood and Cox [1978]. The atmospheric transmissivity is based on Braslau and Dave [1973], which included scattering by H_2O, CO_2, and O_3 as well as an average dust loading. The annual variation of the solar flux received at the surface of the inland North African coast following this estimation is illustrated in Figure 14.

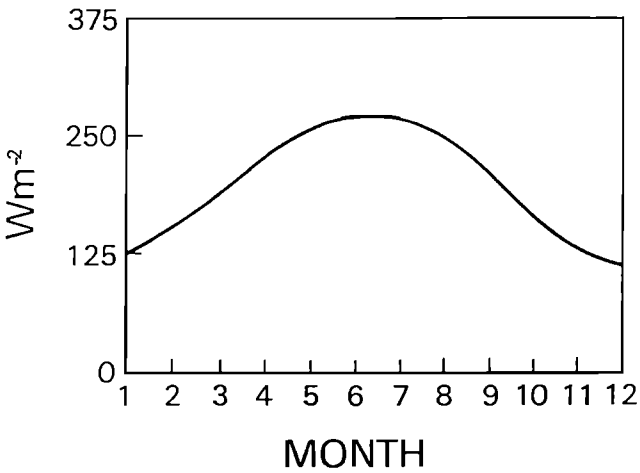

Fig. 14. The annual change of the solar flux received at the surface of the North African coast. Values are in watts per square meter.

Although the net emission of infrared radiation from the surface could be as large as 20-40% of the available solar energy S, the major part of this energy, about 75% [Wallace and Hobbs, 1977, p. 321], is absorbed in the lower troposphere (by CO_2, H_2O, and dust particles). The net emission of the IR radiation from the surface is therefore assumed to be redistributed in the lower troposphere. For simplification, this contribution is assumed to be a fraction of the sensible heat flux and distributed in the same form. Also, as the flux into the ground is only about 3% and the latent heat flux is close to zero [see Ackerman and Cox 1982], the energy is distributed exponentially by the dry convection, with a scale height of h. The diabatic heating due to the surface sensible heat flux at a given altitude Z is therefore

$$Q(Z) = S_o \exp(-Z/h) \qquad (9)$$

where S_o is the diabatic heating at the surface. Following Dòös [1961], we have also assumed h = 3.75 km, and the sensitivity to this choice is discussed later. The value of S_o was obtained by the requirement that the total sensible heating through the atmosphere should equal S. This leads to

$$S_o = \rho_o\ Sh\left(\frac{1}{h} - \frac{1}{H}\right) \qquad (10)$$

where ρ_o is the air density at the surface and H is the atmospheric scale height (H = 8 km). The amount of diabatic heating $\Delta T(Z)$ at the altitude Z is then given by

$$\Delta T(Z) = c_p\ S_o \exp(-Z/h) \qquad (11)$$

It should be mentioned that the diabatic heating in the model was based on a diurnal calculation of the sensible heat flux, since to the first order of magnitude the typical time scale of the Sharav Cyclone, as evidenced by observations, is 1 day (see Table 1).

The value of h = 3.75 km agrees well with evidence for deep dry convection over the desert. Indications for that are the large amounts of desert dust which reach altitudes of 4-5 km [see Blake, 1983]. Charney [1975] has also assumed a convection depth of 5 km over the Sahara through the whole year. Values of diabatic heating $\Delta T(Z)$ for April calculated from (11) are listed in Table 2 for different h values: 1.5, 2.5, and 3.75 km, and at the mandatory pressure levels up to 500 mbar. The results indicate that for h = 2.5 km the heating at 700 mbar was decreased by only 0.4 K. But a further decrease of h to 1.5 km would have resulted in more significant changes.

TABLE 2. Diabatic Heating ΔT in April Due to Sensible Heat Flux for Pressure Levels of 1000, 850, 700, and 500 mbar for h = 1.5, 2.5, and 3.75 km

	Pressure, mbar			
h, km	1000	850	700	500
1.5	13.2	4.9	1.8	0.3
2.5	8.8	4.8	2.6	0.9
3.75	6.6	4.4	3.0	1.4

Values of ΔT are in degrees Kelvin per day. Values were calculated from equation (11).

4.2.2. The static stability parameter and the thermal wind. According to the definition of the static stability σ, the additional heating by $\Delta T(Z)$ decreases σ and increases λ and therefore increases the growth rate and the speed of the cyclone (equation (8)). It should be mentioned that the heating ΔT was divided by 2, since typically, half of the cyclone is above the sea, where ΔT is assumed to be zero. Of course, it would be more realistic to confine the heating to the land half of the cyclone, but this is not possible in the current model.

The increase in the thermal wind is the result of the additional heating $\Delta T(Z)$ only above land. The additional thermal wind will be approximated from

$$\frac{\partial T}{\partial y} \sim \frac{\Delta T}{\Delta y}$$

where Δy is the north to south "mixing scale" across the coast between the cool Mediterranean air mass and the hot desert air (see Figure 15). A mixing scale of 1000 km was assumed, following Charney [1975]. This value is also in agreement

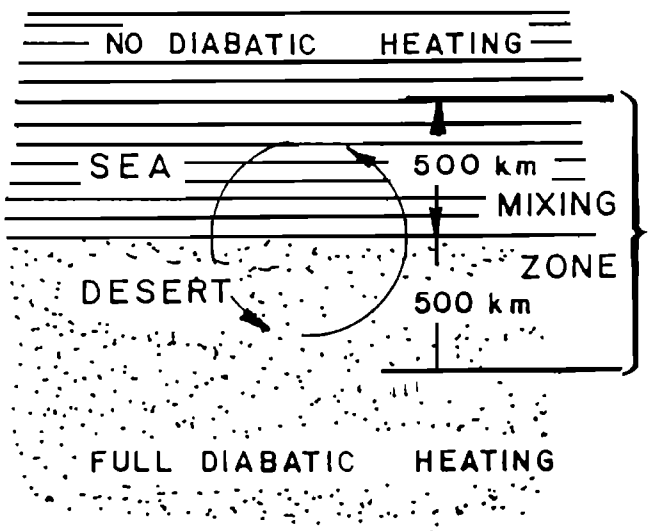

Fig. 15. A schematic representation of the North African coastline and the mixing zone.

with the horizontal scale of the Sharav Cyclone (Table 1). The "mixing scale" was further increased by the distance traveled in 1 day with a speed v, where v is the north to south climatological wind component at 850 mbar. This has increased y from 1000 to 1250 km through the period from June to September, when the average northerly wind speed is 5 m s^{-1}. Following the thermal wind relation

$$\frac{\partial u}{\partial \ln p} = -\frac{R}{f}\frac{\partial T}{\partial y} \qquad (12)$$

and the definition of U_T as 1/2 (U_1 - U_3) (see equation (3)), one finds that

$$\Delta U_T = \frac{1}{2}\frac{\Delta p}{p}\frac{R}{f_o}\frac{\Delta T}{\Delta y} \qquad (13)$$

For instance, in an average month of April, ΔT at the 700-mbar level is 3 K; $\Delta y = 10^3$ km, Δp = 300 mbar, and p = 700 mbar have resulted in $\Delta U_T \sim 2.5$ m s^{-1}. Since the climatological value for the thermal wind at 700 mbar is 6.5 m s^{-1}, the estimated increase due to the sensible heat flux amounts to 38%. When this is added to the climatological value, the growth rate increases by about 45%.

Table 3 summarizes the annual change of the diabatic heating rates calculated from (11) at the mandatory pressure levels up to 500 mbar and the modifications induced in the static stability parameter and the thermal wind U_T. The full list of Cairo's climatological data employed in this study is given in Table 5.

5. Results and Discussion

5.1. Growth Rates and Cyclogenesis

Figure 16 shows the annual change of the maximum growth rate, (equation (7)), for baroclinic disturbances over the Egyptian coast.

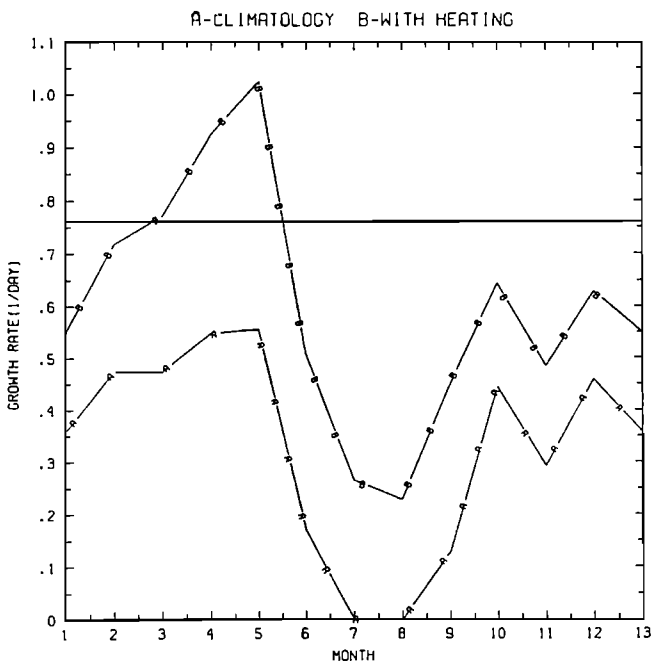

Fig. 16. The annual change of the maximum growth rate (per day): curve A shows climatological data over the North African coast from equation (7) and Cairo's data; curve B shows curve A modified with diabatic heating. Horizontal line at 0.76 per day represents critical value estimated from the Ekman boundary layer pumping.

Curve B represents the growth rate values with the effects of the diabatic heating incorporated, while curve A is the model result when only climatological data has been used. The annual maximum for the cyclogenetic activity is during spring (April-May) and the secondary maximum is in winter (December). A third maximum is in October. The unmodified e-folding time for the maximum growth rate in April is 1.75 days, and it drops to 1 day (i.e. higher growth rate) when the diabatic heating is included. It is interesting to note that the maximum growth rate in April is nearly double that of winter for the North African coast.

During the winter period (November-February) the diabatic heating rates at 700 mbar drop below

TABLE 3. Annual Change of Diabatic Heating Rates ΔT at the Mandatory Pressure Levels up to 500 mbar and the Modifications Induced in σ and U_T

	Month											
	1	2	3	4	5	6	7	8	9	10	11	12
Absorbed Energy, cal cm^{-2} d^{-1}	260	310	400	480	530	540	540	510	440	350	280	240
Diurnal diabatic heating, K d^{-1}												
500 mbar	0.8	0.9	1.2	1.4	1.5	1.6	1.6	1.5	1.3	1.0	0.9	0.7
700 mbar	1.6	1.9	2.5	3.0	3.3	3.3	3.3	3.2	2.8	2.2	1.8	1.5
850 mbar	2.4	2.8	3.7	4.4	4.9	4.9	4.7	4.7	4.0	3.2	2.6	2.2
1000 mbar	3.6	4.3	5.5	6.6	7.3	7.3	7.3	7.0	6.1	4.8	3.8	3.3
Climatology U_T, m s^{-1}	5.6	6.5	6.5	6.5	5.8	3.7	2.4	2.2	3.6	6.0	5.2	7.0
$U_T + \Delta U_T$, m s^{-1}	7.0	8.1	8.6	9.0	8.6	5.9	4.6	4.3	5.6	7.4	6.6	8.3
Climatological σ, (kg^{-2} m^4 s^2) x 10^{-6}	2.0	1.9	1.9	1.6	1.3	1.8	2.2	2.2	1.9	1.8	2.1	2.2
Modified σ, (kg^{-2} m^4 s^2) x 10^{-6}	1.8	1.6	1.6	1.3	1.0	1.5	1.9	1.9	1.6	1.6	1.9	2.0

2 K d^{-1}, a value which comes close to the radiative values of the diabatic heating that were neglected. Also, in this period the intensive winter cyclones frequently tend to destroy the local north to south temperature gradient. We have therefore neglected the diabatic heating contribution in winter. Figure 17 presents curve B, for which diabatic heating smaller than 2 K d^{-1} (at 700 mbar) was neglected. For comparison, curve A, identical to curve B of Figure 16, is shown as well. The spring maximum is now remarkable. The summer values are the smallest, and the secondary maximum is in October. This result corresponds well with frequencies of cyclonic occurrences over the North African coast. However, the friction at the boundary layer and the spindown effect draw energy from the developing cyclone, which causes it to lose power quickly, and these mechanisms were not considered. The rate of the cyclone decay due to this effect is estimated for a barotropic disturbance by (see, for example, Holton, [1979])

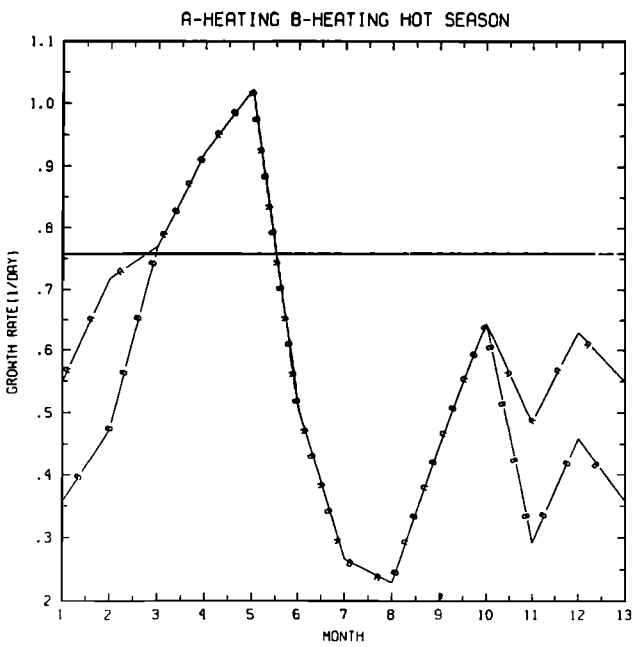

Fig. 17. As in Figure 16, but curve A is with heating through the year, while curve B is modified. For explanation, see text.

$$\frac{1}{\tau_d} = \left[fK/2(H_t - De)^2\right]^{0.5} \qquad (14)$$

where K is the turbulent diffusivity, H_t the cyclone vertical scale, and De is the depth of the boundary layer. On substitution of De = 1.5 km, H_t = 6.5 km, f = 7.3 × 10^{-5} s^{-1}, and K = 50 m^2 s^{-1}, one gets 0.76 per day, or a decay time τ_d of 1.3 days. The relatively high value for K corresponds to the vigorous heat and momentum fluxes at the desert boundary layer, adopted as well by Charney [1975]. The development of Sharav Cyclones therefore needs growth rates which exceed some critical value, as, for instance, 0.76. Figure 17 indicates that such is the case only from March to May. But, since our estimation for τ_d is crude (e.g., the barotropic assumption in deriving τ_d) the secondary maximum in September-October, which is below this critical value, could still be realized as an indication for the Sharav Cyclones during the autumn, which occur only about once in a month. In contrast, during April the average number of Sharav Cyclones is 4-5 (see, for example, Weather in the Mediterranean, [1962]).

It should be emphasized that strictly speaking, theoretical growth rates should be compared to observed intensification rates. However, the generation of the Sharav Cyclone is primarily a consequence of a lee effect of the Atlas Mountains and is not within the scope of the present study. Here our concern is in the maintenance mechanisms of the cyclones on their long track along the North African coast. Hence it was assumed that the growth rates can represent the capability of the baroclinic instability mechanism to maintain and advance the Sharav Cyclone against the dissipation mechanisms.

5.2. Physical Interpretation of Diabatic Heating Contributions to the Sharav Cyclone

Following our model assumptions, the Sharav Cyclone extracts its energy from the baroclinicity of the basic state. The diabatic heating acts directly as an energy source, through the change in the static stability, and, in addition, enhances baroclinicity by increasing the thermal wind of the basic state. Table 4 presents the April growth rates with and without the contribution due to the diabatic heating for convection depths of h = 1.5, 2.5, and 3.75 km.

TABLE 4. April Growth Rates With and Without Contributions by Diabatic Heating for Convection Depths h = 1.5, 2.5, and 3.75 km

	Growth Rate, days		
	h=1.5	h=2.5	h=3.75
Climatology only	0.57	0.57	0.57
With diabatic heating			
With σ correction only	0.74	0.70	0.67
U_T correction only	0.72	0.80	0.83
Both σ and U_T corrections	0.92	0.96	0.98

The convection depth does not alter significantly the increase of the growth rate when diabatic heating effects are included. However, there are significant changes in the relative contribution of the two effects. As the convection becomes shallower, the heating of the 700-mbar level decreases and the thermal wind contribution decreases. But, the enhanced heating at the lower level increases the instability and its contribution through σ. For realistic values of the convection height (h = 2.5 and 3.75 km), the baroclinic contribution is dominant.

5.3. Speed of the Sharav Cyclone

Cohen et al. [1976] have suggested that the Sharav Cyclone moves eastward with a speed which is 70% of the wind at 500 mbar. The present model relates its speed to U_m, which is the average wind intensity between 850 and 550 mbar. This relation is given by (8):

$$c = U_m - \frac{\beta}{\lambda^2} \frac{(y + 1)}{y(y + 2)}$$

The increase of instability (lower σ) increases λ^2, resulting in a higher speed c. Hence the diabatic heating contributes to increase the Sharav Cyclone speed. The speed value in April is 7.9, while 70% of the 500-mbar speed is larger, that is, 13.3 m s^{-1}. The observed speed is above 10 m s^{-1}, and the model therefore underestimates the cyclone's speed.

An interesting result is the fact that c is much larger in April, 7.9 m s^{-1} as compared to June (3.7 m s^{-1}) or October (2.7 m s^{-1}). This is in agreement with observations and results mainly from the large difference in the climatological input speeds, but also from the larger stability in June and October relative to April (see Table 5).

5.4. Cutoff Wavelengths

Up to this point, we have only considered the growth rates and speeds for wavelengths with the maximum growth rates. The growth rates as a function of the wavelength for January through October are described in Figure 18. The short cutoff determines the minimum wavelength that could become unstable. The shortest is obtained in May. Also, the wavelength with maximum growth rate in May is the shortest, that is, ~2600 km, while in January it is the largest. The large difference in the wavelength between April-May and January might indicate the observed large difference in the horizontal scale between the Sharav Cyclone and the winter cyclone (Table 1).

6. Summary

The two-level baroclinic model results based on climatological input from North Africa lend support to the supposition that the Sharav Cyclone is basically the result of a classic baroclinic instability. The synoptic baroclinicity represented by the average thermal wind at the North African coast turned out to be insufficient in explaining the high frequency of occurrence of the Sharav Cyclone. However, when the low-level baroclinicity due to the sea-land contrast was added, a stronger spring maximum was obtained. The model may explain some of the unique features of the Sharav Cyclones at the North African coast: (1) They develop primarily in spring and are less frequent in October. (2) Their horizontal scale is relatively small. (3) They move fast.

However, the speed in which the cyclone moves eastward is in general even larger than that obtained in the model. It could be explained by the fact that the cyclone is often positioned in a region where upper level velocities are higher than the climatological averages employed as the model input. The model seems to indicate that the

TABLE 5. Monthly Climatological Data for Wind and Temperature of Cairo Soundings That Served as Model Input

	Month											
	1	2	3	4	5	6	7	8	9	10	11	12
Zonal wind speed, m s^{-1}												
$\underline{U}_{500}$	18.0	20.0	20.0	19.0	16.5	12.0	5.5	5.0	8.5	13.0	13.0	18.5
$U_1 = \left(\frac{3}{4}U_{500} + \frac{1}{4}U_{700}\right)$	15.7	17.6	17.6	17.0	14.6	10.4	4.8	4.3	7.3	11.1	10.9	16.1
$U_2 - U_{700}$	9.0	10.5	10.5	11.0	9.0	5.5	2.5	2.0	3.5	5.5	4.5	9.0
$U_3 = U_{850}$	4.5	4.5	4.5	4.0	3.0	3.0	0	0	0	0.8	0.5	2.0
$U_M = \frac{1}{2}(U_1\ U_3)$	10.1	11.0	11.0	10.5	8.8	6.7	2.4	2.2	3.6	6.0	5.7	9.0
$U_T = \frac{1}{2}(U_1 - U_3)$	5.6	6.5	6.5	6.5	5.8	3.7	2.4	2.2	3.6	5.1	5.2	7.0
Temperature, °C												
T_{500}	-18	-17	-16	-14	-11	-7	-2	-3	-6	-11	-14	-15
T_{700}	-2	0	+1	+4	+8	+11	+13	+12	+11	+7	+3	+1
T_{850}	+6	+8	+10	+14	+18	+19	+21	+20	+19	+16	+10	+8
Potential temperature, K												
Θ_{500}	311	313	314	316	319	324	330	329	326	320	316	315
Θ_{700}	300	303	304	307	311	315	317	316	314	310	306	304
Θ_{850}	292	295	296	301	306	306	308	307	307	303	296	294
Static stability parameter σ, (kg^{-2} m^4 s^2) x 10^6	2.0	1.9	1.9	1.6	1.3	1.8	2.2	2.2	1.9	1.8	2.1	2.2

Data base supplied by the Government of Israel, for the years 1968-1978.

autumn Sharav Cyclones are much slower than those in the spring. Another feature not explained by the model is the nearly constant structure and speed of the cyclone. It could be the result of the quite uniform basic state along the North African coast, particularly due to the lower layer baroclinicity, which supports both the unstable environment and the counteracting dissipation processes and therefore keeps the cyclone in a quasi-steady situation.

It should be mentioned that sometimes Sharav Cyclones become active and are then associated with precipitation, thunderstorms, etc. These mid-latitude-type cyclones are believed to be associated with an intrusion of a strong polar jet stream into the North African region and tend to occur in early spring [see Tantawy, 1964]. In order to explain the precipitating Sharav Cyclones, the model must be modified, primarily by adding diabatic heating due to latent heat release and by redefining the basic state, which differs greatly from that given by the climatological data.

The Sharav Cyclone's cross sections shown in this study, for April 28-29, 1986, indicate, however, that even nonprecipitating Sharav Cyclones are deep tropospheric circulations and that indirect transverse circulations at the exit region of the jet exists and may play an important role that should be further investigated. The center of these transverse circulations lowered with time (from 550 to 700 mbar) and tended to separate from the parent Genoa Cyclone.

In general, the Sharav Cyclone could be treated on three different scales: (1) the larger global scale introduced in the model by the climatological data, which change from month to month; (2) the regional mesoscale of the order of 1000 km and 1 day, which is strongly modified by the boundary layer forcing of the North African coast and introduced in the model by the diabatic heating; and (3) the smaller local scale (meso-'beta') of the order of 100 km and 1 hour. In the present study the smaller scale in which one has also to deal, for example, with the frontal structure of the Sharav Cyclone, was not considered.

Currently, the model is modified to include explicitly the effects of the boundary layer as friction, in the form of an Ekman pumping and diabatic heating. Moreover, the radiative heating due to the absorption by the dust will be incorporated to better understand the effects of the dust on the dynamical structure of the cyclone. This is particularly important in the frequent cases where the atmosphere is heavily laden with dust.

Acknowledgments. This study was partially supported by the Bi-National U.S.-Israel Science Foundation, project number 8600230. The authors

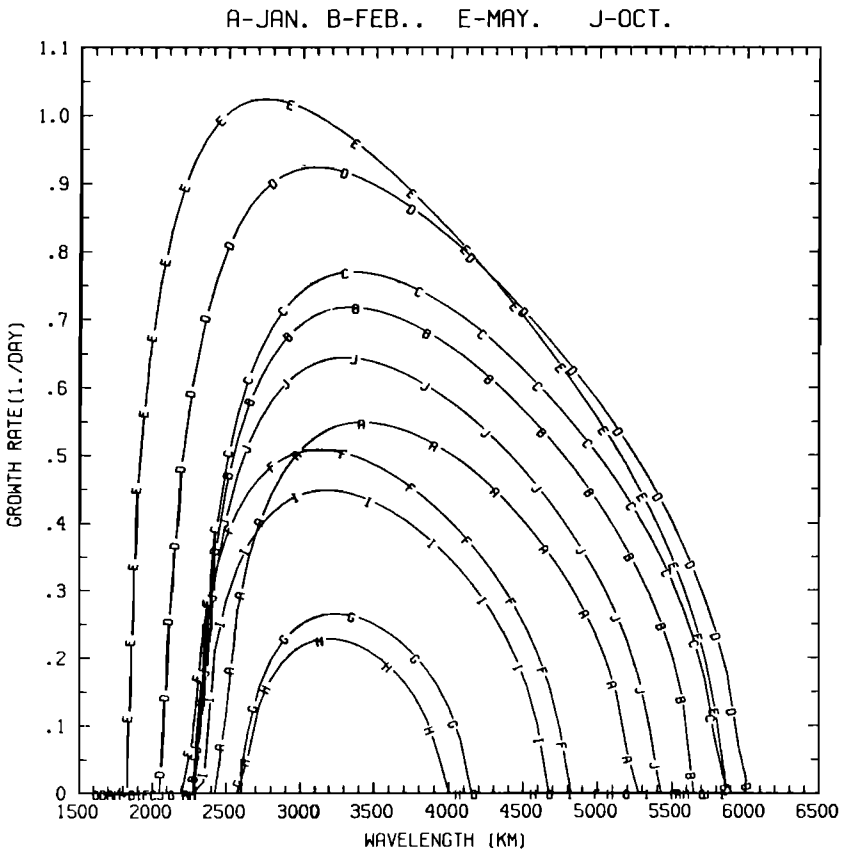

Fig. 18. Growth rates (per day), as function of wavelength for January through October.

wish to thank the Israel Meteorological Service for supplying us with the data. Special thanks go to L. Uccellini and D. Keyser for very helpful suggestions, particularly regarding the jet stream effect. Also, we thank G. Sommeria, ECMWF, for the cross sections; Aharon Dvir, for drafting the figures; Rachel Duani, for her nice typing; and S. Rehavi, for the computing assistance.

References

Ackerman, S. A., and S. K. Cox, The Saudi-Arabian heat flow: Aerosol distribution and thermodynamic structure, J.Geophys. Res. 87, 8991-9002, 1982.

Bengtsson, L., M. Kanamitsu, P. Kallberg, and S. Uppala, FGGE 4-dimensional data assimilation at ECMWF, Bull. Am. Meteorol. Soc., 63, 29-43, 1982.

Blake, P. W., Heat low over the Saudi-Arabian desert during May 1979, Mon. Weather Rev., 111, 1759-1775, 1983.

Braslau, N., and J. V. Dave, Effects of aerosols on the transfer of solar energy through realistic model atmospheres, J. Appl. Meteorol., 12, 601-619, 1973.

Brill, K. F., L. W. Uccellini, R. P. Burkhart, T. T. Warner, and R. A. Anthes, Numerical simulations of a transverse indirect circulation and low-level jet in the exit region of an upper level jet, J. Atmos. Sci., 42, 1306-1320, 1985.

Charney, J. G., Dynamics of desert and drought in the Sahel, Q. J. R. Meteorol. Soc., 101, 193-202, 1975.

Cohen, A., N. Wolfson and M. Graber, Physics and Dynamics of the Atmosphere (in Hebrew), 232 pp., Academon, Hebrew University, Jerusalem, 1976.

Döös, B. R., The scale of non-adiabatic heating as a factor in cyclogenesis, J. Meteorol., 18, 1-8,1961.

Druyan, L. M., North African cyclonic systems and springtime temperatures in Israel, Israel Meteorol. Res. Pap., vol. II, pp. 244-255, Israel Meteorol. Serv., Tel Aviv, 1978.

Elfandy, M. G., The formation of depressions of the Khamsin type, Q. J. R. Meteorol. Soc., 66, 325-335, 1940.

Holton, J. R., An Introduction to Dynamic Meteorology, 2nd ed., 391 pp., Academic, San Diego, Calif., 1979.

Lee, I. Y., Simulation of transport and removal processes of the Saharan dust, J. Clim. Appl. Meteorol., 22, 632-639, 1983.

Liou, K. N., An Introduction to Atmospheric Radiation, Academic, San Diego, Calif., 1980.

Pedgley, D. E., Desert depressions over north-east Africa, Meteorol. Mag., 101, 228-243, 1972.

Phillips, N. A., Energy transformations and meridional circulations associated with simple baroclinic waves in a two-level, quasi-geostrophic model, Tellus, 6, 273-286, 1954.

Reiter, E. R., Handbook for forecasters in the

Mediterranean, Tech. Pap. 5-75, 344 pp., Nav. Postgrad. Sch., Monterey, Calif., 1975.

Rockwood, A. A., and S. K. Cox, Satellite IR surface albedo over north-western Africa, J. Atmos. Sci., 35, 513-522, 1978.

Stone, P. H., Baroclinic adjustment, J. Atmos. Sci., 35, 561-571, 1978.

Tantawy, A. H. I., The role of the jet stream in the formation of desert depressions in the Middle East, WMO Tech. Note 64, 159-171, World Meteorol. Organ., Geneva, Switzerland, 1964.

Tantawy, A. H. I., On the cyclogenesis and structure of spring Sahara depressions in subtropical Africa, Meteorol. Res. Bull., 69, pp. 68-107, Dep. of Meteorol., United Arab Republic, Cairo, 1969.

Wallace, J. M., and P. V. Hobbs, Atmospheric Science: An Introductory Survey, 46 pp., Academic, San Diego, Calif., 1977.

Weather in the Mediterranean, 2nd ed., vol. 1, 362 pp., Her Majesty's Stationery Office, London, 1962.

Westphal, D. L., O. B. Toon and T. N. Carlson, A Numerical Investigation of Saharan Dust Storms, Ph.D. thesis, Penn. State Univ., University Park, 1985.

Winstanley, D., Sharav, Weather, 27, 146-160, 1972.

P. Alpert and B. Ziv, Department of Geophysics and Planetary Sciences, Tel Aviv University, Ramat Aviv 69978, Israel.

(Received February 16, 1988;
revised October 15, 1988;
accepted December 7, 1988.)